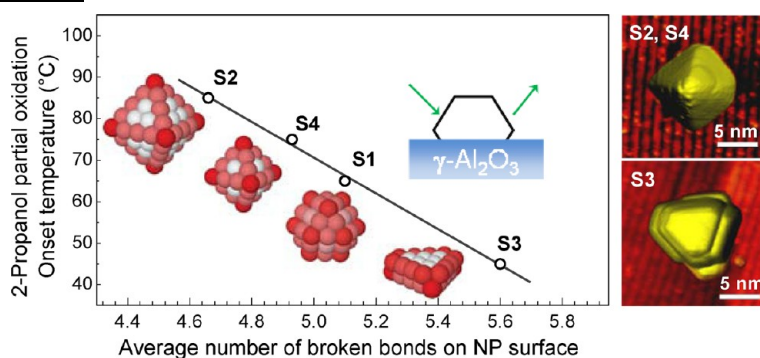# Metal Nanoparticle Catalysts Beginning to Shape-up

BEATRIZ ROLDAN CUENYA*

Department of Physics, University of Central Florida, Orlando, Florida 32816, United States

CONSPECTUS

The field of heterogeneous catalysis has received a remarkable amount of interest from scientific and industrial perspectives because of its enormous impact on the world's economy: more than 90% of chemical manufacturing processes use catalysts. Catalysts are also essential in converting hazardous waste into less harmful products (car exhaust) and in generating power (fuel cells). Yet in all applications, it remains a challenge to design long lasting, highly active, selective, and environmentally friendly catalytic materials and processes, ideally based on Earth-abundant elements. In addition, the field needs more satisfactory experimental and theoretical approaches to minimize trial and error experiments in catalyst development.

Nanocatalysis is one area that is developing rapidly. Researchers have reported striking novel catalytic properties, including greatly enhanced reactivities and selectivities, for nanocatalysts compared to their bulk counterparts. Fully harnessing the power of nanocatalysts requires detailed understanding of the origin of their enhanced performance at the atomic level, which in turn requires fundamental knowledge of the geometric and electronic structures of these complex systems.

Numerous studies report on the properties that affect the catalytic performance of metal naoparticles (NPs) such as their size, interaction with their support, and their oxidation state. Much less research elucidates the role played by the NP shape. Complicating the analysis is that the preceding parameters are not independent, since NP size and support will affect which NP shapes are most stable. In addition, we must consider the dynamic nature of NP catalysts and their response to the environment, since the working state of a NP catalyst might not be the state in which the catalyst was prepared, but rather a structural and/or chemical isomer that responded to the particular reaction conditions. In order to address the complexity of real-world catalysts, researchers must undertake a synergistic approach, taking advantage of a variety of in situ and operando experimental methods. With the continuous shrinking of the scale of material systems, researchers require more sensitive experimental probes and computational approaches that work across a wide range of temperatures and chemical environments.

This Account provides examples of recent advances in the preparation and characterization of NP catalysts with well-defined shapes. It discusses how to resolve the shape of nanometer-sized catalysts via a combination of microscopy and spectroscopic approaches, and how to follow their evolution in the course of a chemical reaction. Finally, it highlights that, for structure-sensitive reactions, controlled synthesis can tune catalytic properties such as the reaction rates, onset reaction temperature, activity, and selectivity.

Introduction

Greatly enhanced reactivities and selectivities have been reported for nanoparticle (NP) catalysts as compared to their bulk counterparts,[1-9] and numerous experimental studies have focused on correlating catalytic activity with NP size, composition, and support.[1-6,8] Nevertheless, although it has also been recognized that the NP shape is an important parameter of consideration,[1,4,10-28] insufficient information

is still available on the most stable shapes for common catalytic materials, how they are affected by the NP size and support, as well as their evolution in the course of a chemical reaction.

Since different crystallographic facets can be stabilized on NPs with different shapes, different reactivities and selectivities may be expected on distinct facets. For example, nanocube Ag NPs with {100} facets were found to be 14 times more active for the oxidation of styrene than nanoplates, and 4 times more active than spherical NPs.[17] A similar trend was reported for the selective epoxidation of ethylene over Ag nanostructures, with nanocubes and nanowires with predominantly {100} facets displaying better selectivities than nanospheres composed mainly of {111} facets.[27] A shape-dependent reactivity was also observed for Cu_2O nanocrystals, with {111} facets being photocatalytically active when interacting with negatively charged molecules, and cubes with {100} facets being inert.[21] With the help of these methods. the larger fraction of corner and edge atoms present in tetrahedral Pt NPs as compared to cubic NPs was also held responsible for the lower activation energy and faster dissolution of surface Pt atoms during the reaction between hexacyanoferrate (III) and thiosulfate ions.[16] The effect of the NP shape on the oxygen reduction reaction (ORR) over Pt NPs was investigated.[18] Based on the distinct electrocatalytic activities observed for differently oriented NP arrays, a synergistic cooperative behavior for ORR between {100} and {111} facets was suggested, with O_2 preferentially adsorbing on (100) facets, but subsequently diffusing to {111} facets where it is more efficiently reduced.[18] The selectivity of hydrogenation reactions could also be tuned by selecting Pt nanocatalysts with different shapes.[29] In particular, Pt nanocubes with {100} planes displayed enhanced selectivity for the conversion of benzene to cyclohexane, while a mix of cyclohexane and cyclohexene was obtained over cuboctahedron NPs with {100} and {111} facets.[29] Higher selectivity for *n*-butylamine was observed for Pt nanocubes as compared to nanopolyhedra during the hydrogenation of pyrrole due to their more favorable ring-opening ability.[30] Furthermore, the high selectivity for the thermodynamic unfavorable isomerization of *trans*-2-butene to its *cis* counterpart observed over tetrahedral Pt NPs dispersed on SiO_2-xerogel was assigned to the high content of Pt(111) facets,[25] with more open surfaces [e.g., Pt(110)] leading to the reverse reaction. Furthermore, sample heating resulting in changes in the NP shape and a decrease in the content of Pt(111) facets gave rise to a decrease in *trans*-to-*cis* conversion.[25] Enhanced reactivities and lower onset

temperatures for the oxidation of CO were measured over Pd octahedral and spherical NPs with predominantly {111} facets, as compared to Pd nanocubes with {100} facets.[23] The stronger binding of CO to the {111} facets was considered advantageous for this catalytic oxidation reaction. The above examples illustrate the importance of taking into consideration the NP shape for the understanding of catalytic performance. Nevertheless, it should also be noted that structure-insensitivity, for example, reaction rates and product distributions independent of the NP size and shape, has also been reported for a variety of catalytic reactions[31−33] and, in some instances, for the same reactions over different catalytic materials or under distinct reaction conditions.[33−35]

While electron-beam lithography has been used in the past to generate catalysts with well-defined structures,[18] its high cost, lack of scalability, and the limitation in the minimum NP size which can be achieved using this method makes it undesirable for a large number of structure-sensitive catalytic processes. Colloidal chemistry approaches have been proven to be a valuable alternative, since they also result in uniform NP size distributions for smaller NP sizes.[1,29,36] Size-selection is crucial in order to ensure homogeneity of the NP shape distributions.[37] Nevertheless, despite significant recent activity in this area,[8,9,11,14,16,17,21,36] challenges still remain in the synthesis of shape-selected colloidal NPs < 5−7 nm. Additionally, despite possibly well-defined initial NP structures (size and shape), NP catalysts should be viewed as dynamical entities which might be subject to structural, morphological, as well as chemical changes under reaction conditions.[10,38] True understanding of structure−reactivity correlations can only be achieved if the evolution of the catalyst geometry is monitored under operando conditions. For this purpose, experimental facilities including advanced in situ synchrotron spectroscopy and scattering, high pressure X-ray photoelectron spectroscopy (HP-XPS), electron microscopy and diffraction, as well as first principle theoretical calculations under realistic environments must be considered.[4,5,7,10,18,39−43] For instance, the dynamic response of supported Pd NP catalysts to CO/NO cycles in terms of changes in the NP size, shape, and composition was recently reported.[44] Furthermore, the morphology and equilibrium shape of Pd and Rh nanocrystals was found to be modified upon O_2 adsorption, with closed-packed (111) facets being mainly present under low O_2 pressures, and (110) open surfaces leading to nanocrystal rounding dominating at elevated pressures.[42] An increase in the total area of (100) facets at the expense of (111) surfaces was observed for Rh NPs upon oxidation, a change which
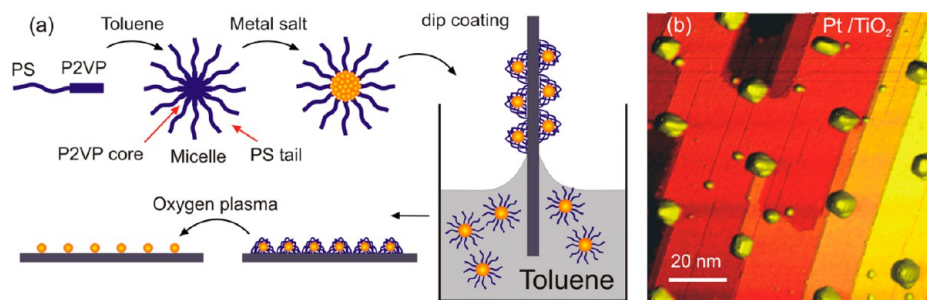
FIGURE 1. (a) Schematic description of the inverse micelle encapsulation NP synthesis. (b) STM image of Pt NPs on TiO$_2$(110) acquired at RT after sample heating in UHV at 1000 °C.

could be reversed upon subsequent NP reduction.[45] High resolution transmission electron microscopy (TEM) images obtained under H$_2$ and O$_2$ atmospheres demonstrated the faceting of TiO$_2$-supported Au NPs under H$_2$ (truncated octahedron shape), and their rounding and dewetting under O$_2$.[46] Chemisorption-induced morphological changes in NPs such as the ones described above need to be considered when models to explain catalytic reactivity are proposed, since certain reaction environments might lead to a decrease/increase in the relative area of the most catalytically active surface facets/sites.

The above description emphasizes the need of not only having a thorough knowledge of the average NP size and size distribution characteristic of a particular sample, but also the most stable NP shapes under any given set of reaction conditions (temperature, pressure, chemical environment), since both parameters will affect chemical reactivity. Although such studies have already been initiated, significant additional effort will be needed in the years to come to address changes in the NP structure under a certain chemical or reaction environment and take advantage of such knowledge in the rational design of the next generation of nanoscale catalysts.

Colloidal Synthesis of Size- and Shape-Selected Nanoparticles

New approaches for the fabrication of nanostructures based on inverse micelle encapsulation methods have enabled our group to produce model catalyst samples with narrow NP size and shape distributions as well as uniform arrangements over large surface areas.[1,37,47−50] Figure 1a shows a schematic of the process used to generate submonolayer coverages of self-assembled NPs. It involves the dissolution of diblock copolymers (PS-P2VP) in toluene leading to the formation of inverse micelles, the loading of the micelles with a metal salt precursor (e.g., H$_2$PtCl$_6$, HAuCl$_4$, FeCl$_3$), dip-coating of the desired thin film or single crystal support into the polymeric solution, and subsequent ligand removal in ultrahigh vacuum (UHV) by means of an O$_2$/H$_2$ plasma treatment. The NP size can be tuned
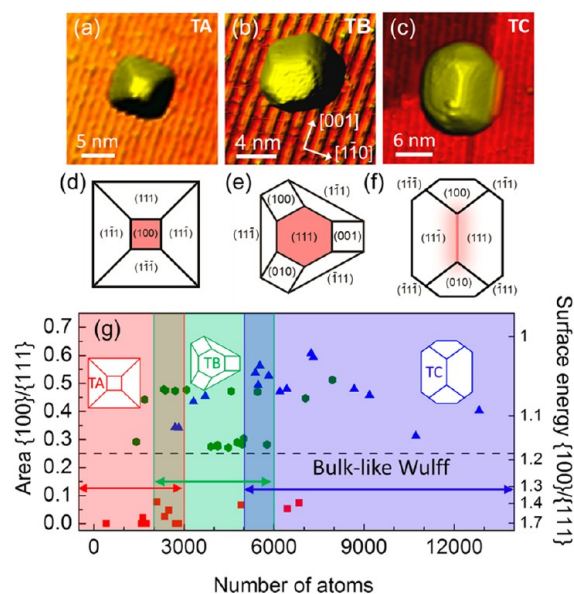

FIGURE 2. (a−c) STM images of micellar Pt NPs on TiO$_2$(110) taken at RT after heating in UHV above 1000 °C. The facet orientations within each shape are shown in (d−f). Three size regimes featuring different NP shapes were found. (g) Ratio of surface areas and energies of {100} versus {111} facets as a function of the NP size (or number of atoms within the NP).

by changing the length of the polymer head (P2VP) or the metal/P2VP ratio, while the interparticle distance can be controlled by changing the length of the polymer tail (PS).

Solving the Structure of Nanoparticles: STM and EXAFS

The scanning tunneling microscopy (STM) image in Figure 1b corresponds to Pt NPs on TiO$_2$(110) prepared using this micelle-based synthesis and was acquired after sample heating in UHV at 1000 °C and subsequent cooling to room temperature (RT). A remarkable thermal stability of the micellar NPs is evidenced by the preservation of the original hexagonal arrangement and lack of changes in the average NP height.[47] Furthermore, the high temperature annealing treatment was found to lead to geometrically well-defined
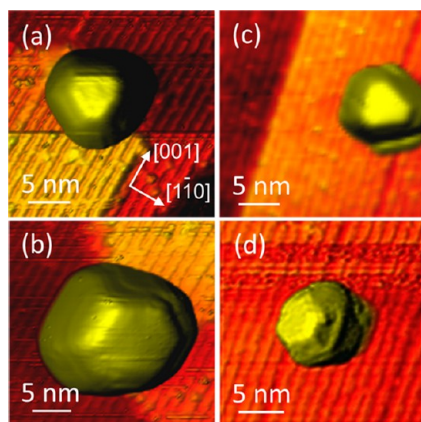
FIGURE 3. STM images of micelle-synthesized Au (a, b) and Pt (c, d) NPs on TiO$_2$(110) acquired at RT after heating in UHV above 1000 °C.

FIGURE 4. (a) Overlap between the lattices of a Pt(100) interfacial facet and the TiO$_2$(110) surface shown as a function of the strain (ε_x) parallel to [001] and the in-plane rotation angle of the Pt(100) lattice with respect to the TiO$_2$(110)-[001] direction. The strain (ε_y) was fixed to the optimum value of -6.4% giving rise to the maximum Pt/TiO$_2$ lattice overlap. The strain is defined as ($L_{bulk} - L_{relaxed})/L_{bulk}$, where L_{bulk} and $L_{relaxed}$ are the lattice parameters of bulk platinum and the strained Pt structure, respectively. A negative strain shows the expansion of the Pt lattice at the NP/support interface. These calculations assume that only the Pt lattice is strained to adapt to the TiO$_2$ lattice underneath the NPs, while the TiO$_2$ lattice is assumed to remain rigid.

3D faceted Pt NPs in their equilibrium state, Figure 2a−f. Our study also demonstrated that the initial NP volume can provide a means to control the final NP shape, with three main shape categories being stable for the micelle-synthesized Pt NPs on TiO$_2$(110), Figure 2g. Besides, the shapes of these NPs were found to differ from the kinetically limited shapes of conventional physical vapor deposited (PVD) NPs, which normally form two-dimensional flat islands on TiO$_2$ upon annealing at elevated temperatures. Moreover, an epitaxial relationship with the TiO$_2$(110) support was observed for the micelle-synthesized Pt and Au NPs.[50] Despite the significant anisotropic interfacial strain present in the former systems, symmetric single crystal NPs were obtained, Figures 2a−c and 3. However, in most cases, the ratio of {100}/{111} facet areas and related surface energies of the NP shapes resolved was found to deviate from that of bulklike Wulff structures, Figure 2g. This is assigned to interfacial strain, not considered in the model *unsupported* Wulff NPs. The epitaxial orientation of the interfacial facets observed via STM and rare occurrence of rotated NPs can be explained based on calculations of lattice mismatch between a given interfacial Pt facet and the TiO$_2$-(110) surface, Figure 4. The majority of our NPs was found to have at least one edge parallel to the TiO$_2$(110)-[100] rows.[37,50] Nevertheless, some rotated NPs were also observed, but those had at least one of their symmetry axes parallel to such rows. The calculations displayed in Figure 4a correspond to a NP of type A (TA) shape (see Figure 2a, d) with a Pt(100) facet in contact with TiO$_2$. Strain coefficients ε of about 6% along the [1$\bar{1}$0] direction of the TiO$_2$(110) surface and -6% along [001] resulted here in the best overlap of the Pt and TiO$_2$ lattices. Nonetheless, it should be noted that such values are likely overestimated, since they assume a rigid TiO$_2$ lattice underneath the NP, and only compression/expansion of the Pt NP
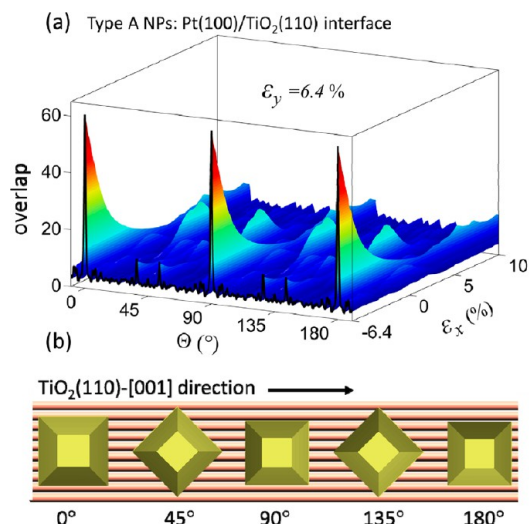
interface. Further theoretical work is needed for such systems in order to gain additional quantitative insight into the extent of the interfacial strain, and how far away from the NP/support interface would the effect still be noticeable within the NP.

The previous examples demonstrate that control over the NP size, shape, dispersion on the support, and interfacial epitaxy can be gained by our colloidal synthesis method, presenting significant advantages toward the rational engineering of active nanoscale catalysts. Furthermore, the thermodynamically stable morphology of our NPs (shapes adopted after thermal treatments at/above 1000 °C and subsequent quenching) guarantees the stability of these material systems under extreme thermal treatments in vacuum, and provides an excellent platform for comparisons with theoretical calculations based on equilibrium NP shapes.[26] It should be however mentioned that for other environments (e.g., H$_2$, O$_2$) different shapes might be more stable. Moreover, these thermally stable NPs with reduced mobility were found to stabilize step edges of the underlying TiO$_2$(110) support, resulting in the formation of TiO$_2$ nanostripes along [001] upon heating in vacuum at elevated temperatures, Figure 5. This result is due to desorption of oxygen and the concomitant diffusion of Ti^{3+} cations perpendicular to the surface into the bulk of TiO$_2$(110).[51] Our finding opens the possibility of using metallic
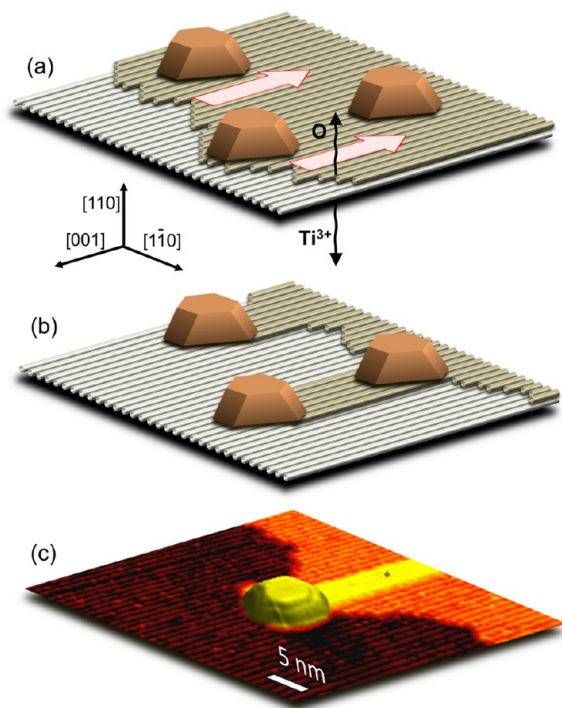
FIGURE 5. (a,b) Schematic representation of the formation of TiO_2 nanostripes stabilized by micellar Pt NPs. Oxygen desorption and inward diffusion of Ti^{3+} (into the bulk of TiO_2) predominantly occurs at [1−10] step edges, while [001] steps remain stable. This results in the loss of unpinned TiO_2 rows starting from their free ends. Pt NPs can stabilize [1−10] steps and protect TiO_2 rows attached to them by those steps. The STM image in (c) displays a nanostripe−nanoparticle configuration.

FIGURE 6. (a) EXAFS data in *r*-space of ∼1 nm Pt NPs/γ-Al_2O_3 with two different shapes (S2, S3). The measurements were done under H_2 atmosphere at RT after NP reduction at 375 °C. Data from a Pt foil are also shown for reference. The insets in (a) correspond to model NP shapes with coordination numbers in agreement with those extracted from the EXAFS data. (b) Coordination numbers (CNs) from 1st to 4th nearest neighbor extracted from the MS analysis of EXAFS data (solid symbols) of S2 and S3 compared to those obtained from model fcc NP shapes with a diameter identical to that of the experimental samples (1.0 ± 0.2 nm) (open symbols). (c) TEM image of ∼1 nm micelle synthesized Pt NPs supported on γ-Al_2O_3 (S2).

micelle-synthesized NPs to pattern catalytically active oxide surfaces, generating uniform arrays of oxide nanostripes with tunable width (related to the NP diameter), orientation, and interstripe distance (related to the interparticle distance).

The above synthesis method is also suitable for the generation of metal NP catalysts on high surface area powder supports.[1,48,52,53] In such cases, the encapsulating ligands are removed by thermal treatments in O_2 at/above 375 °C, and the overall NP shape can be tuned from three-dimensional (3D) to 2D by decreasing the metal loading inside a given micellar cage, with low loadings leading to flatter (2D) NPs.[37,49] The small size and homogeneity of the resulting nanoscale catalysts, Figure 6c, makes them ideal targets for combined operando spectroscopic studies, including extended X-ray absorption fine-structure spectroscopy (EXAFS), diffuse reflectance infrared Fourier transform spectroscopy (DRIFTS), and mass spectroscopy. Although the shape of 3D NPs with sizes above ∼1.5 nm can be resolved via STM (and in some cases atomic force microscopy, AFM), tip-convolution effects prevent the visualization of much smaller
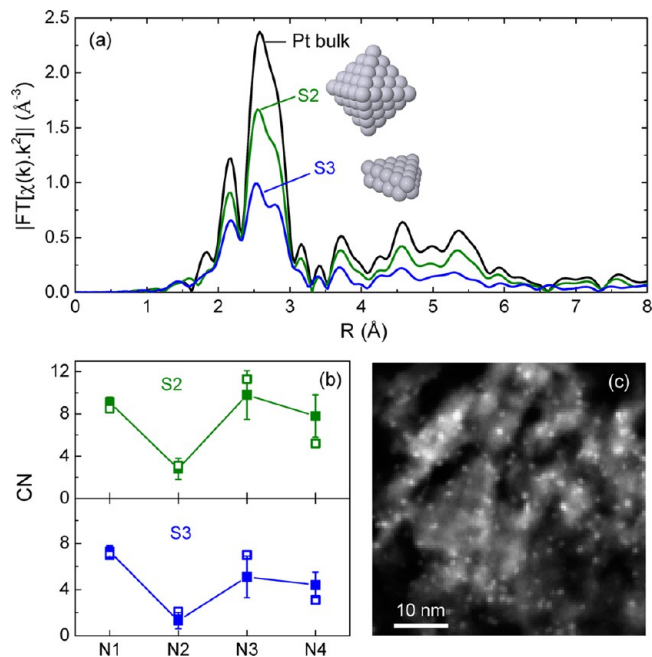
3D NP structures, which appear "spherical" in STM and AFM images. In order to resolve the size and shape of smaller NPs, spectroscopic approaches must be undertaken. We have resolved the structure of small ($0.7 \text{ nm} < d < 1.5 \text{ nm}$) size-selected Pt NPs synthesized by inverse micelle encapsulation by a synergistic combination of TEM, EXAFS (providing average coordination numbers, CNs), and NP shape modeling, Figure 6a, b.[37,48] Figure 6a displays Fourier transform EXAFS spectra corresponding to two Pt NP/γ-Al_2O_3 samples with an average TEM diameter of 1.0 ± 0.2 nm but distinct shape measured at RT in hydrogen. A multiple scattering (MS) analysis of these data led to the experimental 1st−4th nearest neighbor (NN) CNs shown in Figure 6b (closed symbols).[49] The final model NP shapes representative of a given sample (see insets in Figure 6a) were selected from a database of fcc NP shapes based on their agreement with the EXAFS coordination numbers (1st to 4th NN), the TEM NP diameters, and their resemblance to real but larger NP shapes observed by STM on similarly synthesized samples supported on single crystal substrates.
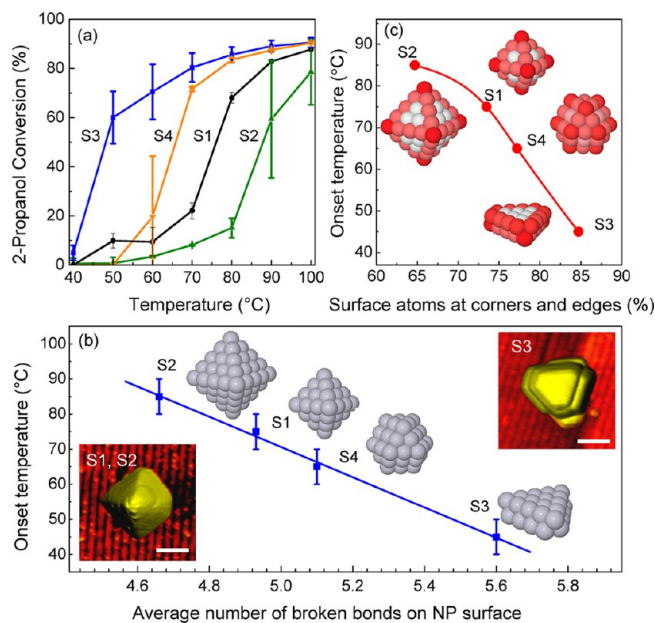
FIGURE 7. (a) Partial oxidation of 2-propanol over Pt NPs of similar size (~0.8 nm S1, ~1 nm S2, S3, S4) but different shape. Onset reaction temperature versus (b) the relative content of atoms at corner and edge sites on the NP surface and (c) the average number of broken bonds at the NP surface. The insets in (b) display the model shapes that best describe the NPs in each of the samples (obtained from EXAFS and TEM measurements and modeling). The color coding of the atoms in (b) reflects different number of nearest neighbors, with the atoms in white having a CN of 9, and those in dark red a CN of 4. The STM images in (c) were acquired on similarly synthesized but larger Pt NPs supported on $TiO_2(110)$.

Structure, Chemical State, and Reactivity Correlations

Shape Effects. Using γ-Al_2O_3-supported micellar Pt NPs with similar size (~0.8 nm for S1 and ~1 nm for S2, S3, S4) but different shape as model systems, the partial oxidation of 2-propanol was investigated in a packed-bed mass flow reactor,[2] Figure 7a. A correlation between the NP shape and the onset reaction temperature was observed, with the bilayer (2D) Pt NPs in S3 displaying the best catalytic performance, Figure 7b.[48] This result suggests that the NP support (γ-Al_2O_3) might play a positive role in the reactivity of these NPs either by inducing strain (the smallest Pt−Pt distances were measured for this sample via EXAFS), by providing catalytically active reaction sites at the NP/support interface (perimeter atoms), or via NP/support charge transfer processes. Nevertheless, the NPs in sample S3 were also the ones with the highest number of low-coordinated atoms, Figure 7b, and among those, corner and edge sites were found to be the most reactive, Figure 7c. As was mentioned before, even though the shapes of these small micelle-synthesized Pt NPs were determined after their stabilization
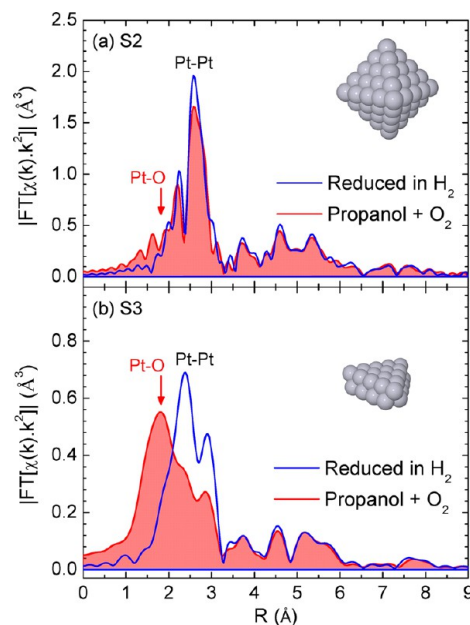

FIGURE 8. k^2-Weighted EXAFS data in r-space obtained from (a) S2 and (b) S3 containing Pt NPs supported on γ-Al_2O_3. The spectra were acquired at RT after sample reduction in H_2 and after subsequent in situ exposure to a mix of O_2 and 2-propanol at RT.
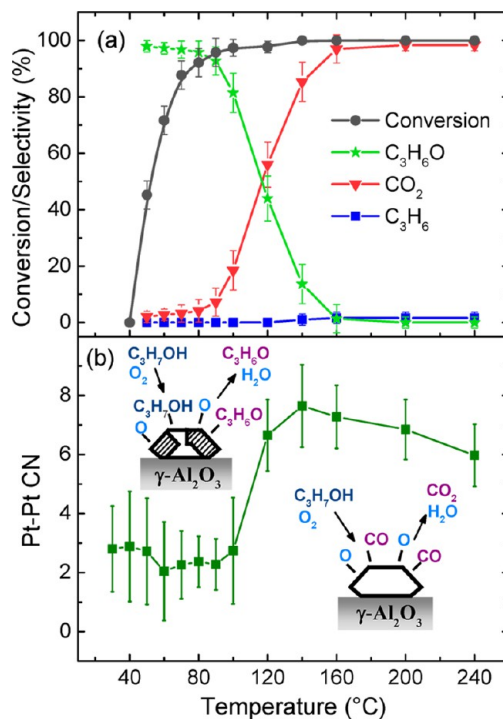

FIGURE 9. (a) Conversion and selectivity data as a function of temperature for the oxidation of 2-propanol over Pt NPs/γ-Al_2O_3. (b) Dependence of the 1st nearest-neighbor coordination number of Pt−Pt metallic species on the reaction temperature obtained from in situ EXAFS spectra. A decrease in the Pt−Pt CN with respect to the as-prepared sample in H_2 (7.1 ± 0.5) indicates the formation of PtO_x species. The change in the selectivity from partial oxidation to complete oxidations occurs at the onset of PtO_x decomposition (~110 °C).
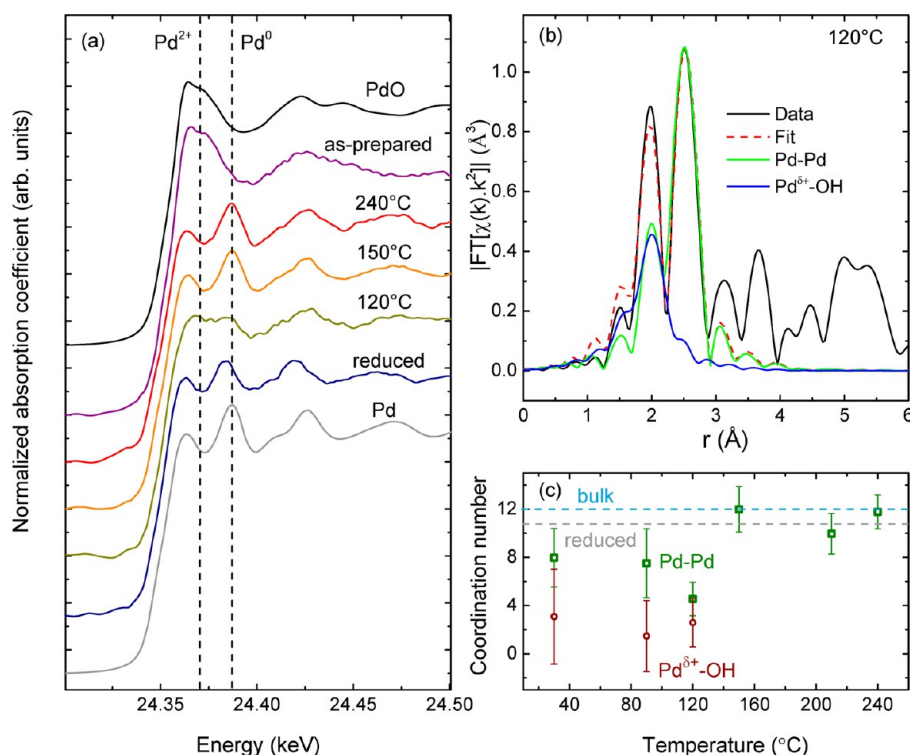
FIGURE 10. (a) Pd K-edge XANES spectra of micelle-synthesized Pd NPs on ZrO_2 taken after polymer removal in O_2 at 375 °C (as-prepared), after reduction in H_2 at 240 °C and subsequent cooling to RT (reduced), and at different temperatures during the NO reduction with H_2. (b) Fourier transform Pd K-edge EXAFS spectrum (*r*-space) recorded at 120 °C in NO + H_2, along with the total fit and the Pd−Pd and $Pd^{\delta+}$−OH contribution. (c) Dependence of the 1st NN CN extracted from EXAFS data on the reaction temperature during the reduction of NO with H_2. The dashed gray line indicates the Pd−Pd CN after NP reduction in H_2 and before reactant exposure.

by prolonged heating treatments in O_2 at 375 °C (24 h) and subsequent reduction in H_2, and the current catalytic reaction was only conducted up to 100 °C, changes in the initial NP shape (models shown as inset in Figure 7b) under reaction conditions cannot be ruled out. Nevertheless, for NPs as small as 1 nm, a study monitoring such changes in situ is extremely challenging, and at present unachievable by most experimental techniques. For example, the high quality EXAFS data required to resolve the shape of small NPs (CNs up to the fourth NN extracted from MS fits are needed to decrease the degeneracy in the possible NP shapes) can only be obtained at or below room temperature, since with increasing temperature disorder effects lead to a decrease in the overall signal intensity and enhanced noise/signal ratios. Additionally, in an oxidizing environment such as the one considered here, not only changes in the NP shape due to O_2 and propanol chemisorption must be considered, but also the oxidation of the Pt NP catalysts, which should also be size-dependent, and might lead to drastic structural changes. Despite these inherent experimental difficulties, we were able to follow changes in the chemical state of the former catalysts during the oxidation of propanol via EXAFS.

Although for the former reasons no detailed information on the NP shape could be obtained under operando conditions, the overall NP size (extracted from the first NN CNs of first-shell EXAFS fits) was found to remain constant during this reaction. However, NPs of identical average size (∼1 nm TEM diameter) but different initial (as-prepared) shape were found to display a distinct reactivity toward O_2, with 2D NPs (S3) being able to dissociate oxygen and become oxidized at RT under propanol and oxygen flow, while only minimum oxidation was observed for the 3D NPs (S2) under analogous conditions,[48] Figure 8. Since our oxidized 2D NPs were the ones displaying the lowest onset reaction temperature under steady-state reaction conditions, PtOx species are suggested to constitute the active phase for the partial oxidation of propanol to acetone, possibly via a Mars−van Krevelen reaction mechanism, where the consumed oxygen from the oxidized NP shell is continuously replenished by oxygen from the gas phase. According to the literature, 2-propanol is likely adsorbed over the γ-Al_2O_3 surface due to this substrate's acidic nature[54] and subsequently interacts with oxygen atoms chemisorbed on the Pt NPs[55] or as it is proposed here, with oxygen from the oxidized NP surface.
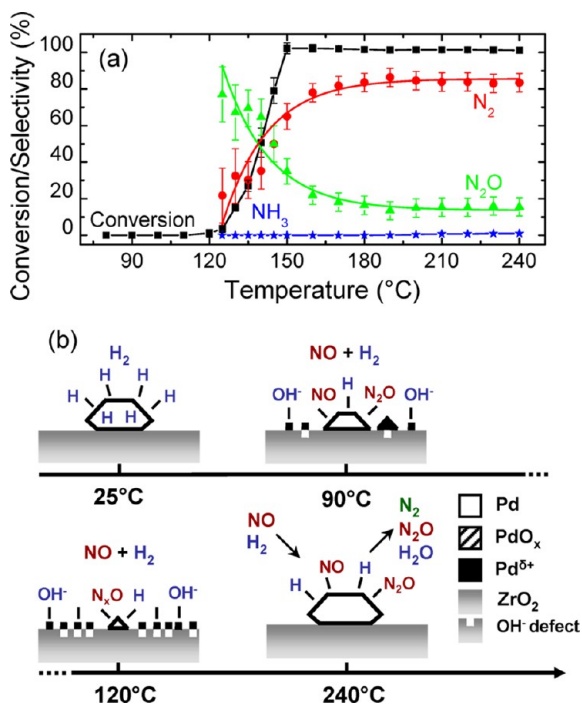
FIGURE 11. (a) Conversion and selectivity data as a function of temperature for the steady state reduction of NO with H_2 over micelle-synthesized Pd NPs supported on ZrO_2. (b) Schematic representation of the structure and chemical state of the Pd NP catalysts at various stages of the NO +H_2 reaction.

Chemical State Effects. In order to shed light into the role of the chemical state of Pt, which as was shown above is strongly dependent on the NP size and shape, on its reactivity, the partial and total oxidation of 2-propanol over $\sim$0.7 nm Pt NPs was studied under operando conditions,[52] Figure 9. Figure 9b shows the evolution of the Pt–Pt metal first NN CN as a function of the reaction temperature. Upon exposure to the reactants at RT, a drastic decrease in the Pt–Pt CN is observed below 100 °C, and a concomitant increase in the Pt–O CN (not shown here). Our combined EXAFS and mass spectrometry data revealed the presence of PtOx species within the partial oxidation regime, when acetone is being produced with >97% selectivity. In contrast, in the total oxidation regime (>100 °C, CO_2 production), the catalysts are initially metallic, but with the surface covered by chemisorbed oxygen, Figure 9b. With increasing reaction temperature, the NPs showed signs of reoxidation, possibly due to the desorption of passivating carbonaceous species (reaction intermediates). The decomposition of the Pt oxides in the intermediate reaction regime, where partial and total oxidation processes coexist, is attributed to the reducing effect of hydrogen released in the dehydrogenation of 2-propanol and intermediate carbonaceous species available at the onset of the complete oxidation, as well as to the

competition of CO and O_2 for adsorption sites on the NP surface.

Significant changes in the structure and chemical state of Pd NP/ZrO_2 catalysts were also observed during the reduction of NO with H_2 via EXAFS and XPS.[53] In particular, the redispersion of the Pd NPs over the ZrO_2 surface and the formation of small cationic Pd clusters or positively charged ions was observed upon the introduction of the reactants (NO + H_2) at RT until the onset temperature for NO reduction was reached (120 °C). In Figure 10a, X-ray absorption near-edge spectroscopy (XANES) data from the Pd–K edge illustrate the evolution of the chemical state of the Pd catalysts under reaction conditions. XANES, EXAFS, and XPS data[53] indicate the gradual transformation of Pd^0 species to $Pd^{\delta+}$ from RT to 120 °C. EXAFS spectra (Pd–K edge) acquired at the onset of the reaction, Figure 10b, revealed the presence of two distinct Pd species, a Pd–Pd metallic component and a long Pd–O bond ($\sim$2.55 Å) which was assigned to cationic Pd species stabilized at OH defects on the ZrO_2 surface. No PdO_x species were formed under our experimental conditions. In parallel to the presence of cationic Pd on our samples, a high selectivity for N_2O was detected at the onset of the NO reduction reaction ($\geq$120 °C), Figure 11a. As the reaction temperature increases (>150 °C), the selectivity shifts mainly toward N_2 ($\sim$80%). Figure 10c displays the evolution of the first NN CNs of the two Pd species in the course of the reaction. Concomitant with the onset of the NO reduction reaction, the disappearance of the $Pd^{\delta+}$ species and formation of larger metallic Pd aggregates are observed in Figure 10c, evidencing that metallic Pd constitutes the active phase for the H_2-reduction of NO over these catalysts. The details of the proposed reaction mechanism are depicted in Figure 11b.

Conclusions

In summary, although a number of catalytic reactions have been shown to be structure-sensitive, most of the studies published to date compare structural data acquired before and after reaction, and fewer examples are available showing direct structural-reactivity correlations extracted from experimental data acquired under reaction conditions. In this respect, further effort is still needed in the years to come for the development of experimental techniques and reactor cells suitable for the investigation of such correlations on sub-monolayer NP arrays and/or single NPs under operando conditions. Some promising candidates include XAFS, XPS, DRIFTS, and E-TEM due to their versatility and ability to operate, in some cases simul-

taneously, under various chemical environments (e.g., gaseous and liquid phases) and under high pressure conditions. With the help of these methods, the paradigm of rationally designing catalysts that are optimized for a given reaction based on fundamental understanding of their intrinsic geometrical (NPs size, shape) and chemical features (oxidation state, secondary metal, dopants) could become a reality.

BIOGRAPHICAL INFORMATION

Beatriz Roldan Cuenya completed her B.S. in Physics from the University of Oviedo, Spain in 1998. She obtained her Ph.D. from the Department of Physics at the University of Duisburg-Essen (Germany) summa cum laude in 2001. She joined the University of Central Florida (UCF) in 2004 after her postdoctoral research in the Department of Chemical Engineering at the University of California Santa Barbara (2001−2003). Currently, she is a professor in the Department of Physics at UCF. Her research program explores novel physical and chemical properties of size- and shape-selected nanostructures, with emphasis on advancements in nanocatalysis.

FOOTNOTES

*E-mail: roldan@ucf.edu.
The authors declare no competing financial interest.

REFERENCES

1 Roldan Cuenya, B. Synthesis and catalytic properties of metal nanoparticles: Size, shape, support, composition, and oxidation state effects. *Thin Solid Films* **2010**, *518*, 3127–3150.

2 Campbell, C. T. The active site in nanopaticle gold catalysis. *Science* **2004**, *306*, 234–235.

3 Freund, H.-J. Model Studies in Heterogeneous Catalysis. *Chem.—Eur. J.* **2010**, *16*, 9384–9397.

4 Hansen, P. L.; Wagner, J. B.; Helveg, S.; Rostrup-Nielsen, J. R.; Clausen, B. S.; Topsoe, H. Atom-resolved imaging of dynamic shape changes in supported copper nanocrystals. *Science* **2002**, *295*, 2053–2055.

5 Nørskov, J. K.; Bligaard, T.; Rossmeis, J.; Christensen, C. H. Towards the computational design of solid catalysts. *Nat. Chem.* **2009**, *1*, 37–46.

6 Grabow, L. C.; Mavrikakis, M. Nanocatalysis beyond the Gold-Rush Era. *Angew. Chem., Int. Ed.* **2008**, *47*, 7390–7392.

7 Vang, R. T.; Lauritsen, J. V.; Laegsgaard, E.; Besenbacher, F. Scanning tunneling microscopy as a tool to study catalytically relevant model systems. *Chem. Soc. Rev.* **2008**, *37*, 2191–2203.

8 Zaera, F. New Challenges in Heterogeneous Catalysis for the 21st Century. *Catal. Lett.* **2012**, *142*, 501–516.

9 Tao, A. R.; Habas, S.; Yang, P. Shape Control of Colloidal Metal Nanocrystals. *Small* **2008**, *4*, 310–325.

10 Newton, M. A. Dynamic adsorbate/reaction induced structural change of supported metal nanoparticles: heterogeneous catalysis and beyond. *Chem. Soc. Rev.* **2008**, *37*, 2644–2657.

11 Crespo-Quesada, M.; Yarulin, A.; Jin, M.; Xia, Y.; Kiwi-Minsker, L. The structure sensitivity of alkynol hydrogenation on shape- and size-controlled Pd nanocrystals: Which sites are most active and selective? *J. Am. Chem. Soc.* **2011**, *133*, 12787–12794.

12 Enterkin, J. A.; Poeppelmeier, K. R.; Marks, L. D. Oriented Catalytic Platinum Nanoparticles on High Surface Area Strontium Titanate Nanocuboids. *Nano Lett.* **2011**, *11*, 993–997.

13 Van Aert, S.; Batenburg, K. J.; Rossell, M. D.; Erni, R.; Van Tendeloo, G. Three-dimensional atomic imaging of crystalline nanoparticles. *Nature* **2011**, *470*, 374–377.

14 Xia, Y. N.; Jin, M. S.; Zhang, H.; Xie, Z. X. Palladium Concave Nanocubes with High-Index Facets and Their Enhanced Catalytic Properties. *Angew. Chem., Int. Ed.* **2011**, *50*, 7850–7854.

15 Yang, H.; Wu, J. B.; Gross, A. Shape and Composition-Controlled Platinum Alloy Nanocrystals Using Carbon Monoxide as Reducing Agent. *Nano Lett.* **2011**, *11*, 798–802.

16 Narayanan, R.; El-Sayed, M. A. Shape-Dependent Catalytic Activity of Platinum Nanoparticles in Colloidal Solution. *Nano Lett.* **2004**, *4*, 1343–1348.

17 Xu, R.; Wang, D.; Zhang, J.; Li, Y. Shape-dependent catalytic activity of silver nanoparticles for the oxidation of styrene. *Chem.—Asian J.* **2006**, *1*, 888–893.

18 Komanicky, V.; Iddir, H.; Chang, K. C.; Menzel, A.; Karapetrov, G.; Hennessy, D.; Zapol, P.; You, H. Shape-Dependent Activity of Platinum Array Catalyst. *J. Am. Chem. Soc.* **2009**, *131*, 5732–5733.

19 Tian, N.; Zhou, Z.-Y.; Sun, S.-G.; Ding, Y.; Wang, Z. L. Synthesis of tetrahexahedral platinum nanocrystals with high-index facets and high electro-oxidation activity. *Science* **2007**, *316*, 732–735.

20 Yuan, Q.; Zhou, Z.; Zhuang, J.; Wang, X. Tunable Aqueous Phase Synthesis and Shape-dependent Eletrochemical Properties of Rhodium Nanostructures. *Inorg. Chem.* **2010**, *49*, 5515–5521.

21 Kuo, C.-H.; Huang, M. H. Morphologically controlled synthesis of Cu$_2$O nanocrystals and their properties. *Nano Today* **2010**, *5*, 106–116.

22 Karim, A. M.; Prasad, V.; Mpourmpakis, G.; Lonergan, W. W.; Frenkel, A. I.; Chen, J. G.; Vlachos, D. G. Correlating Particle Size and Shape of Supported Ru/Y-Al$_2$O$_3$ with NH$_3$ Decomposition Activity. *J. Am. Chem. Soc.* **2009**, *131*, 12230–12239.

23 Wang, R.; He, H.; Liu, L.-C.; Dai, H.-X.; Zhao, Z. Shape-dependent catalytic activity of palladium nanocrystals for the oxidation of carbon monoxide. *Catal. Sci. Technol.* **2012**, *2*, 575–580.

24 Gong, X.; Yang, Y.; Zhang, L.; Zou, C.; Cai, P.; Chen, G.; Huang, S. Controlled synthesis of Pt nanoparticles via seeding growth and their shape-dependent catalytic activity. *J. Colloid Interface Sci.* **2010**, *352*, 379–385.

25 Lee, I.; Delbecq, F.; Morales, R.; Albiter, M. A.; Zaera, F. Tuning selectivity in catalysis by controlling particle shape. *Nat. Mater.* **2009**, *8*, 132–138.

26 Chepulskii, R. V.; Curtarolo, S. Ab Initio Insights on the Shapes of Platinum Nanocatalysts. *ACS Nano* **2011**, *5*, 247–254.

27 Christopher, P.; Linic, S. Engineering selectivity in heterogeneous catalysis: Ag nanowires as selective ethylene epoxidation catalysts. *J. Am. Chem. Soc.* **2008**, *130*, 11264–11265.

28 Susut, C.; Tong, Y. J. Size-dependent methanol electrooxidation activity of Pt nanoparticles with different shapes. *Electrocatalysis* **2011**, *2*, 75–81.

29 Bratlie, K. M.; Lee, H.; Komvopoulos, K.; Yang, P. D.; Somorjai, G. A. Platinum Nanoparticle Shape Effects on Benzene Hydrogenation Selectivity. *Nano Lett.* **2007**, *7*, 3097–3101.

30 Tsung, C.-K.; Kuhn, J. N.; Huang, W.; Aliga, C.; Hung, L.-I.; Somorjai, G. A.; Yang, P. Sub-10 nm Platinum Nanocrystals with Size and Shape Control: Catalytic Study for Ethylene and Pyrrole Hydrogenation. *J. Am. Chem. Soc.* **2009**, *131*, 5816–5822.

31 Che, M.; Bennett, C. O. The Influence of Particle-Size on the Catalytic Properties of Supported Metals. *Adv. Catal.* **1989**, *36*, 55–172.

32 Somorjai, G. A.; Carrazza, J. Structure sensitivity of catalytic reactions. *Ind. Eng. Chem. Fundam.* **1986**, *25*, 63–69.

33 Van Santen, R. A. Complementary Structure Sensitive and Insensitive Catalytic Relationships. *Acc. Chem. Res.* **2009**, *42*, 57–66.

34 Sasahara, A.; Tamura, H.; Tanaka, K. i. The role of Rh on Pt-based catalysts: structure sensitive NO + H2 reaction on Pt(110) and Pt(100) and structure insensitive reaction on Rh/Pt(110) and Rh/Pt(100). *Catal. Lett.* **1994**, *28*, 161–166.

35 Lin, S. D.; Vannice, M. A. Hydrogenation of Aromatic Hydrocarbons over Supported Pt Catalysts .II. Toluene Hydrogenation. *J. Catal.* **1993**, *143*, 554–562.

36 Lee, H.; Habas, S. E.; Kweskin, S.; Butcher, D.; Somorjai, G. A.; Yang, P. D. Morphological control of catalytically active platinum nanocrystals. *Angew. Chem., Int. Ed.* **2006**, *45*, 7824–7828.

37 Roldan Cuenya, B.; Alcantra Ortigoza, M.; Ono, L. K.; Behafarid, F.; Mostafa, S.; Croy, J. R.; Shafai, G.; Rahman, T. S.; Li, L.; Zhang, Z.; Yang, J. C. Thermodynamic Properties of Pt Nanoparticles: Size, Shape, Support, and Adsorbate Effects. *Phys. Rev. B* **2011**, *84*, 245438.

38 McKenna, K. P.; Shluger, A. L. Shaping the morphology of gold nanoparticles by CO adsorption. *J. Phys. Chem. C* **2007**, *111*, 18848–18852.

39 Si, R.; Flytzani-Stephanopoulos, M. Shape and crystal-plane effects of nanoscale ceria on the activity of Au-CeO$_2$ catalysts for the water-gas shift reaction. *Angew. Chem., Int. Ed.* **2008**, *47*, 2884–2887.

40 Salmeron, M.; Schlogl, R. Ambient pressure photoelectron spectroscopy: A new tool for surface science and nanotechnology. *Surf. Sci. Rep.* **2008**, *63*, 169–199.

41 Nørskov, J. K.; Bligaard, T.; Hvolbæk, B.; Abild-Pedersen, F.; Chorkendorff, I.; Christensen, C. H. The nature of the active site in heterogeneous metal catalysis. *Chem. Soc. Rev.* **2008**, *37*, 2163–2171.

42 Mittendorfer, F.; Seriani, N.; Dubay, O.; Kresse, G. Morphology of mesoscopic Rh and Pd nanoparticles under oxidizing conditions. *Phys. Rev. B* **2007**, *76*, 233413.

43 Oxford, S. M.; Lee, P. L.; Chupas, P. J.; Chapman, K. W.; Kung, M. C.; Kung, H. H. Study of Supported PtCu and PdAu Bimetallic Nanoparticles Using In-Situ X-ray Tools. *J. Phys. Chem. C* **2010**, *114*, 17085–17091.

44 Newton, M. A.; Di Michiel, M.; Kubacka, A.; Fernandez-Garcia, M. Combining Time-Resolved Hard X-ray Diffraction and Diffuse Reflectance Infrared Spectroscopy To Illuminate CO Dissociation and Transient Carbon Storage by Supported Pd Nanoparticles during CO/NO Cycling. *J. Am. Chem. Soc.* **2010**, *132*, 4540–4541.

45 Nolte, P.; Stierle, A.; Jin-Phillip, N. Y.; Kasper, N.; Schulli, T. U.; Dosch, H. Shape Changes of Supported Rh Nanoparticles During Oxidation and Reduction Cycles. *Science* **2008**, *321*, 1654–1658.

46 Giorgio, S.; Cabie, M.; Henry, C. R. Dynamic observations of Au catalysts by environmental electron microscopy. *Gold Bull.* **2008**, *41*, 167–173.

47 Naitabdi, A.; Behafarid, F.; Roldan Cuenya, B. Enhanced Thermal Stability and Nanoparticle-mediated Surface Patterning: Pt/TiO$_2$(110). *Appl. Phys. Lett.* **2009**, *94*, 083102.

48 Mostafa, S.; Behafarid, F.; Croy, J. R.; Ono, L. K.; Li, L.; Yang, J. C.; Frenkel, A. I.; Roldan Cuenya, B. Shape-dependent Catalytic Properties of Pt Nanoparticles. *J. Am. Chem. Soc.* **2010**, *132*, 15714–15719.

49 Roldan Cuenya, B.; Croy, J. R.; Mostafa, S.; Behafarid, F.; Li, L.; Zhang, Z.; Yang, J. C.; Wang, Q.; Frenkel, A. I. Solving the structure of size-selected Pt nanocatalysts synthesized by inverse micelle encapsulation. *J. Am. Chem. Soc.* **2010**, *132*, 8747–8756.

50 Behafarid, F.; Roldan Cuenya, B. Nanoepitaxy Using Micellar Nanoparticles. *Nano Lett.* **2011**, *11*, 5290–5296.

51 Behafarid, F.; Roldan Cuenya, B. Nano pinstripes: TiO$_2$ nanowire formation by nanoparticle-mediated pinning of step edges. *J. Phys. Chem. Lett.* **2012**, *3*, 608–612.

52 Paredis, K.; Ono, L. K.; Mostafa, S.; Li, L.; Zhang, Z. F.; Yang, J. C.; Barrio, L.; Frenkel, A. I.; Roldan Cuenya, B. Structure, Chemical Composition, And Reactivity Correlations during the In Situ Oxidation of 2-Propanol. *J. Am. Chem. Soc.* **2011**, *133*, 6728–6735.

53 Paredis, K.; Ono, L. K.; Behafarid, F.; Zhang, Z. F.; Yang, J. C.; Frenkel, A. I.; Roldan Cuenya, B. Evolution of the Structure and Chemical State of Pd Nanoparticles during the in Situ Catalytic Reduction of NO with H$_2$. *J. Am. Chem. Soc.* **2011**, *133*, 13455–13464.

54 Padilla, J. M.; Del Angel, G.; Navarrete, J. Improved Pd/γ-Al$_2$O$_3$—Ce catalysts for benzene combustion. *Catal. Today* **2008**, *133*—*135*, 541–547.

55 Augustine, R. L.; Doyle, L. K. The Platinum-Catalyzed Oxidation of 2-Propanol. *J. Catal.* **1993**, *141*, 58–70.